SYSTEMS, SCIENCE AND SOFTWARE

SSS-R-79-4023

SMALL-SCALE EXPLOSION EXPERIMENTS, SEISMIC SOURCE CALCULATIONS AND SUMMARY OF CURRENT RESEARCH

P. L. COLEMAN
S. M. DAY
N. RIMER
J. T. CHERRY
J. R. MURPHY
T. C. BACHE

QUARTERLY TECHNICAL REPORT
FOR PERIOD JANUARY 1 - MARCH 31, 1979

SPONSORED BY
ADVANCED RESEARCH PROJECTS AGENCY
ARPA ORDER No. 2551

This research was supported by the Advanced Research Projects Agency of the Department of Defense and was monitored by AFTAC/VSC, Patrick Air Force Base, Florida, 32925, under Contract No. F08606-79-C-0008.

APPROVED FOR PUBLIC RELEASE, UNLIMITED DISTRIBUTION.

MAY 1979

P. O. BOX 1620, LA JOLLA, CALIFORNIA 92038, TELEPHONE (714) 453-0060

AFTAC Project Authorization No. VT/9712/B/PMP

ARPA Order No. 2551, Program Code No. 6H189

Effective Date of Contract: November 17, 1978

Contract Expiration Date: September 30, 1979

Amount of Contract: $847,285

Contract No. F08606-79-C-0008

Principal Investigator and Phone No.
Dr. Thomas C. Bache, (714) 453-0060, Ext. 337

Project Scientist and Phone No.
Captain Michael J. Shore, (202) 325-7581

UNCLASSIFIED

SECURITY CLASSIFICATION OF THIS PAGE (When Data Entered)

REPORT DOCUMENTATION PAGE		READ INSTRUCTIONS BEFORE COMPLETING FORM
1. REPORT NUMBER	2. GOVT ACCESSION NO. AD-A114787	3. RECIPIENT'S CATALOG NUMBER
4. TITLE (and Subtitle) Small-Scale Explosion Experiments, Seismic Source Calculations and Summary of Current Research		5. TYPE OF REPORT & PERIOD COVERED Quarterly Technical 1-1-79 to 3-31-79
		6. PERFORMING ORG. REPORT NUMBER SSS-R-79-4023
7. AUTHOR(s) P. L. Coleman, S. M. Day, N. Rimer, J. T. Cherry, J. R. Murphy, T. C. Bache		8. CONTRACT OR GRANT NUMBER(s) F08606-79-C-0008
9. PERFORMING ORGANIZATION NAME AND ADDRESS Systems, Science and Software P. O. Box 1620 La Jolla, California 92038		10. PROGRAM ELEMENT, PROJECT, TASK AREA & WORK UNIT NUMBERS Program Code No. 6H189 ARPA Order No. 2551
11. CONTROLLING OFFICE NAME AND ADDRESS VELA Seismological Center 312 Montgomery Street Alexandria, Virginia 22314		12. REPORT DATE May 1979
		13. NUMBER OF PAGES 41
14. MONITORING AGENCY NAME & ADDRESS (if different from Controlling Office)		15. SECURITY CLASS. (of this report) Unclassified
		15a. DECLASSIFICATION DOWNGRADING SCHEDULE

16. DISTRIBUTION STATEMENT (of this Report)

Approved for Public Release, Unlimited Distribution.

17. DISTRIBUTION STATEMENT (of the abstract entered in Block 20, if different from Report)

18. SUPPLEMENTARY NOTES

19. KEY WORDS (Continue on reverse side if necessary and identify by block number)

Seismic Source Theory
Nuclear Explosion Seismology

20. ABSTRACT (Continue on reverse side if necessary and identify by block number)

Brief summaries of work currently underway or completed in the period from 1 January to 31 March 1979 are presented. Technical results not previously reported are given in five sections. One describes the development and testing of small spherical charges which will be emplaced in concrete blocks to simulate large explosions in the laboratory. A second section discusses an analysis of the free-field data from the MERLIN event. The

(over)

DD FORM 1 JAN 73 1473 EDITION OF 1 NOV 65 IS OBSOLETE

UNCLASSIFIED

SECURITY CLASSIFICATION OF THIS PAGE (When Data Entered)

ABSTRACT (Continued)

other three sections are concerned with finite difference simulations of explosion and earthquake sources. These include results from calculations of PILEDRIVER and of decoupled explosions in salt. Also described is a fracture criterion for three-dimensional finite difference modeling of earthquake faulting.

TABLE OF CONTENTS

LIST OF ILLUSTRATIONS

I. INTRODUCTION

1.1 BACKGROUND

The objective of the Systems, Science and Software (S^3) research program is to extend our present understanding of the excitation of seismic waves by underground explosions and earthquakes. Toward this objective, we are conducting theoretical and empirical studies of ground motions from the two classes of sources. In particular, our efforts are directed toward the development of improved methods for discriminating between the seismic signals from earthquakes and explosions and the development of improved methods for estimating explosion yield.

This report summarizes the work done during the second three-month period of the contract.

1.2 SUMMARY OF RESEARCH DURING THIS QUARTER

Our work during this quarter has included research in a number of areas. Research projects are briefly summarized below.

Source Calculations

A. Calculations of Nuclear Explosions in Granite

One-dimensional and two-dimensional finite difference calculations of the PILEDRIVER event have been made and are in excellent agreement with the observations. A brief discussion of these calculations is given in Section V. Also discussed in that section are some one-dimensional calculations of the French explosions in the Sahara. In Section VI we discuss some recent calculations of decoupled explosions in salt. The results are in good agreement with the SALMON/STERLING experiment.

B. Earthquake Modeling on the ILLIAC IV Computer

Our earthquake calculations done on the ILLIAC computer have so far included only a rather simple model for the physics of earthquake faulting. The great advantage of the TRES code on the ILLIAC computer is that realistic physics can be incorporated into the model. In Section IV we describe a recently developed algorithm for a three-dimensional numerical treatment of fracture on a fault plane. This model is now being incorporated into the TRES program on the ILLIAC.

Discrimination

During this reporting period we completed the MARS processing for 127 events recorded at the Priority 1 stations. After several attempts, and a recopy of the original tape, we have been unable to convert data for event 149. In addition, we have not received digital seismograms for events 274 through 278 for any of the Priority 2 stations.

Preliminary variable frequency magnitude (VFM) results for the Priority 1 stations were presented at the VSC meeting on April 11, 1979 in Alexandria, Virginia. The degree of separation of earthquakes and presumed explosions appears to be dependent on several factors. In addition to possible spectral differences in the earthquake and explosion source functions, the propagation path in the vicinity of a particular station and the level of background earth noise both contribute to this separation. To date the station RKON, sited on the Canadian shield, has yielded the maximum separation of the presumed explosions from the majority of earthquakes. In contrast, the two event populations exhibit the least amount of separation at the station ANMO, located within the Basin and Range Province. Two reports, describing detailed results from the Priorities 1 and 2 station sets, are in preparation.

Small-Scale Experiments

Recent progress in simulating underground explosions by using small PETN charges in concrete blocks is described in Section II.

Research Activities at the Reston Geophysics Office

The research project includes several tasks being done by J. R. Murphy and his colleagues in our Reston Office. Progress on these tasks is summarized in Section III.

II. SEISMIC MODELING EXPERIMENTS

2.1 INTRODUCTION

The objective of these experiments will be to make measurements of free surface motion due to the detonation of one or more small high explosive (HE) charges within a uniform, well-characterized medium. The data will be used as benchmarks for the finite difference codes used to predict the seismic motions generated by underground explosions. The principal activity to date has been the development and testing of the HE charges; see the discussion below. The initial experiment, designed to check instrument performance and confirm previous measurements, will be conducted by 13 April 1979.

2.2 HE CHARGE DEVELOPMENT

There are four main requirements for the charges:

1. They should be spherical.
2. The power and energy output should be uniform from charge to charge.
3. The performance of the explosive should be well characterized so that the codes can accurately model the detonation.
4. The charges should be small so that a reasonably sized block of the medium (of order one cubic meter) gives elastic motions on its free surfaces.

A few tenths gram of PETN, initiated by an exploding bridgewire and contained within a plastic shell of one centimeter diameter, meets all these requirements. Figure 1 shows some details of construction. The shell is formed from two hemispheres. The bridgewire and its leads are sealed into one hemisphere. A small loading port is cut from the other hemisphere. After the hemispheres are glued together, a

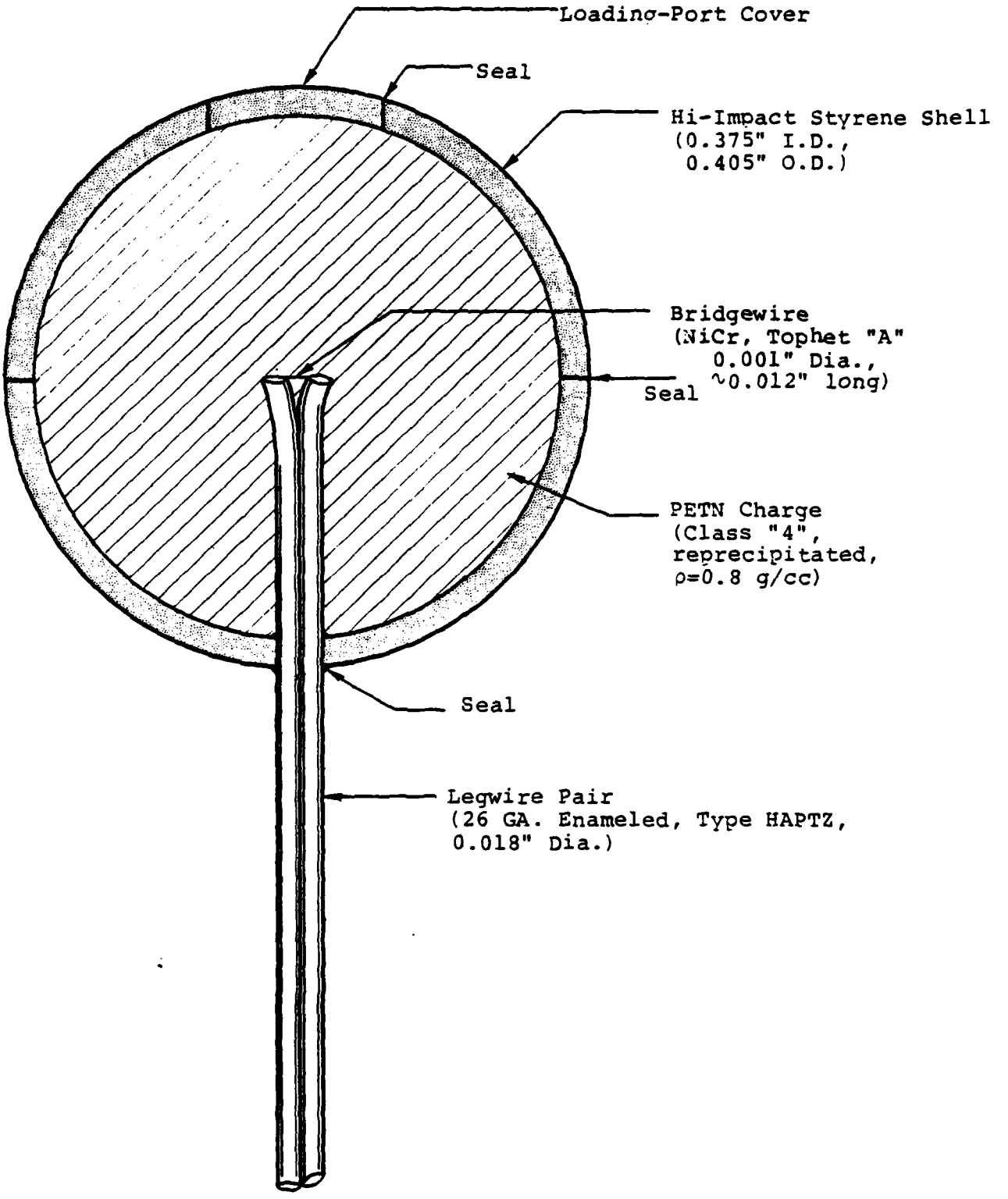

Figure 1. Spherical explosive charge (section view, 10 x scale).

measured amount of PETN powder† is poured into the shell and then the port is sealed in place. All seals are made with styrene solvent cement. This assembly technique ensures accurate centering of the bridgewire and good waterproofing for the explosive.

We evaluated the performance of these charges by detonating them in a small tank of water and photographing the tests with a framing camera operating at about 500,000 frames per second. In order to see both the expansion of the HE and the shock wave in the water, the tank was backlit. Such photographs are essentially shadowgraphs*, thus the ideal light source is a distant, bright point emitter. We approximated the ideal with a commercial photo flash "strobe"** located about one tenth meter behind the four inch cubical water tank. The film was a high speed, high contrast type (Kodak 2475, ASA 1,000) and the effective aperature of the camera was f/28.

We also placed a pressure sensor 20.3 mm from the surface of the HE sphere to measure the water shock. The sensor was a bar gauge type. The actual probe in the water, a one-eight inch diameter, 100 mm long piece of oil-hardened steel drill rod, acoustically transmits the pressure on the end of the rod to the transducer, x-cut quartz.

Some examples of the photographs for the first test on 14 March 1979 are shown in Figure 2. Because the camera cannot by easily synchronized with the high voltage detonating pulse, absolute time is uncertain for each frame. Defining frame 1 as showing first evidence of detonation leads to the timing shown in the figure. Frame -1 shows the unexploded sphere

---

†The mean size of the PETN particles must be small compared to the diameter of the bridgewire (25 μm) to ensure high order detonation of the explosive.

*The HE products are at a temperature about 2500 to 3000°K which makes them weakly self luminous in the red and infrared parts of the spectrum.

**Rated guide number of 60 for a film speed of ASA25.

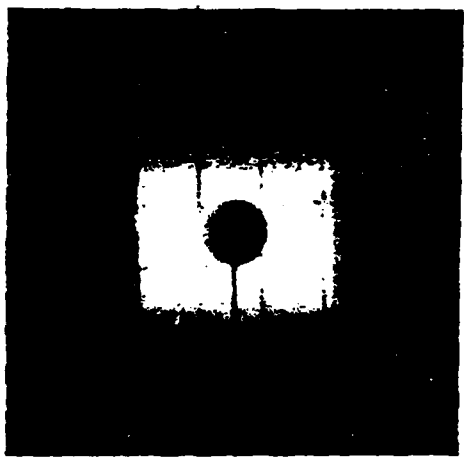

Frame -1
t=-1.9μs

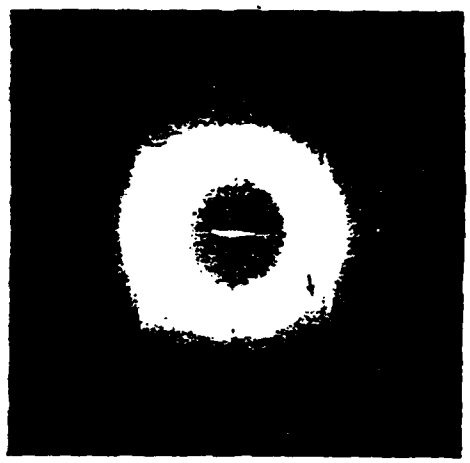

Frame 3
t=5.6μs

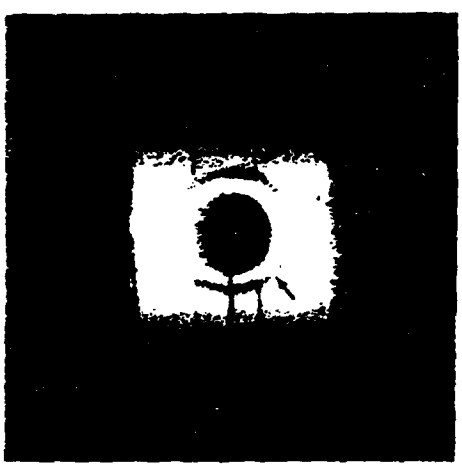

Frame 1
t=1.9μs

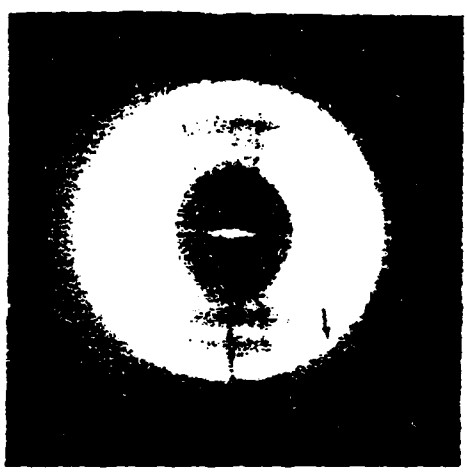

Frame 5
t=9.4μs

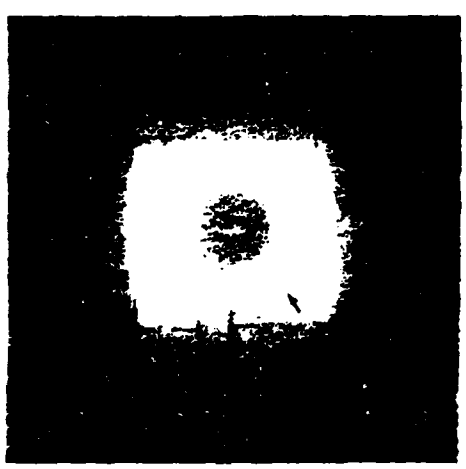

Frame 2
t=3.7μs

Frame 7
t=13.1μs

Figure 2. Framing camera photographs of detonation of HE sphere in water, first test of 14 March 1979. Arrow shows shock front. (Scale x 0.88)

(painted black) supported on its lead wires in front of a 10 mm spacing grid pattern. Expansion of HE gases is evident even in frame 1. Measurements from these prints give an initial water shock velocity of 2.8 mm/μs and a maximum particle velocity (i.e., the HE gas motion) of 0.6 to 0.7 mm/μs. Both velocities are consistent with an initial water shock pressure of 1.8 GPa (18 kbar). Based on a packing density of 0.8 g/cc, the equation of state for PETN (N. Rimer, private communication) also predicts an initial pressure of 1.8 GPa in the HE products. In frame 3, the thin brigh band along the sphere's equator is presumably due to the hot HE products; the joint between the hemispheres is probably thinner than the rest of the shell. In frame 7 the shadow at the top shows that the water shock has moved a few millimeters beyond the end of the bar gauge. By this time, the shock has slowed to 1.7 mm/μs* and the HE products are expanding at 0.4 mm/μs.

Defining asymmetry in percent as

$$\frac{[\text{Polar Diameter}] - [\text{Equatorial Diameter}]}{[\text{Polar Diameter}]} \times 100$$

the HE products show a maximum of three percent asymmetry and the shock, minus five percent, for this test. By 10 μs, both measures were less than one percent. Other tests show similar or smaller asymmetries. The centers of the sphere, expanding HE gases, and water shock are coincident to within a millimeter.

Figure 3 gives a typical pressure record. The finite risetime (1 μs) and ringing after the peak (period of about 2 μs) are characteristics† of a bar subjected to a step function pressure input. This record implies a true shock pressure

*Sonic velocity in water is 1.65 mm/μs.

†Dispersion in the propagation of compressional waves along the bar account for these features.

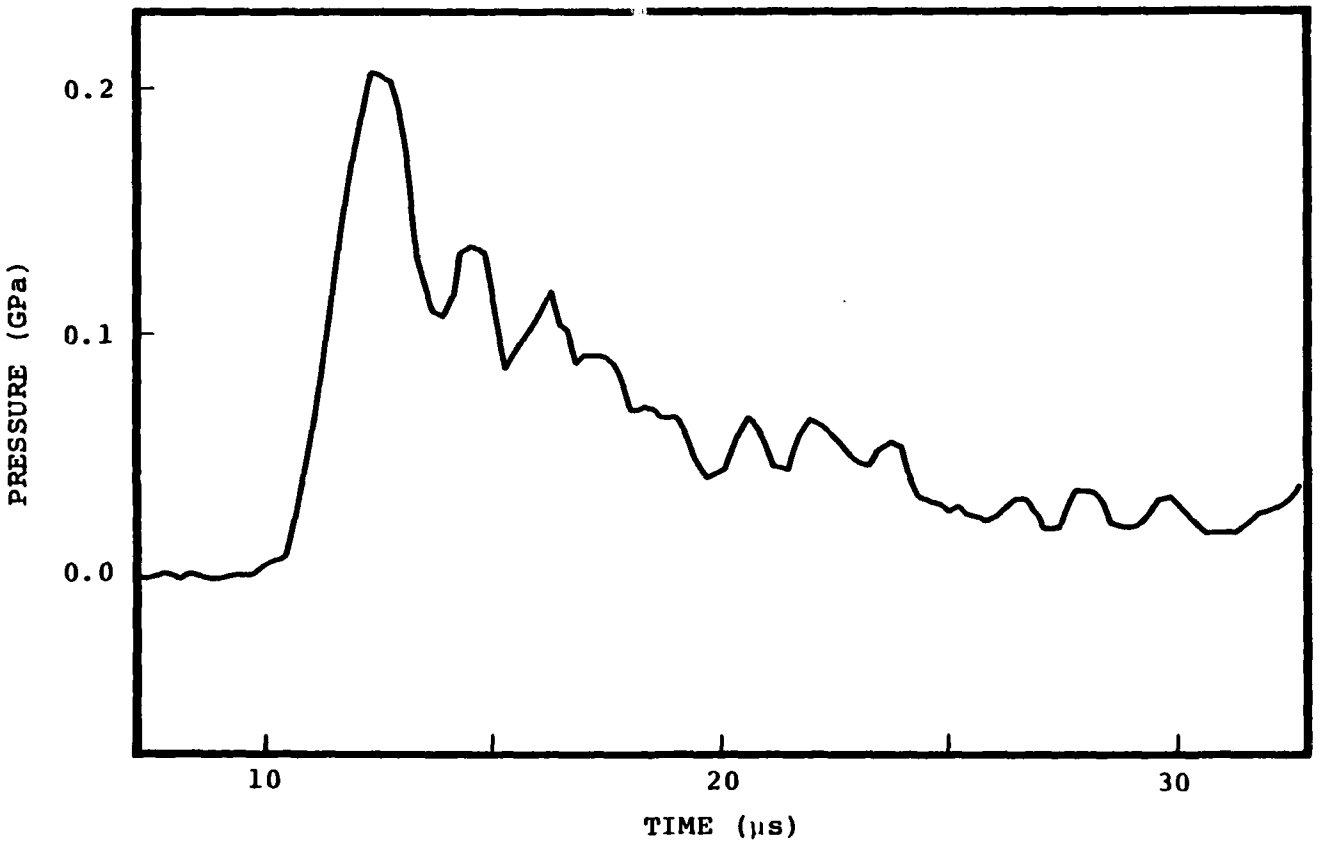

Figure 3. Bar gauge pressure record for water tank test of HE sphere, 14 March 1979.

of 0.2 GPa (2 kilobar) with a submicrosecond rise time and 1/e decay of about 5 μs. These data are consistent with the velocity data from the photographs.

As a result of these tests, we can now generate consistent, symmetric, high-order detonations in small explosive charges. In anticipation of our planned seismic modeling experiments, we will also photograph the simultaneous explosion of two or three charges in a water tank to confirm equal detonation rates between charges.

III. SUMMARY OF RESEARCH ACTIVITIES AT THE RESTON GEOPHYSICS OFFICE

3.1 MAGNITUDE-YIELD IMPROVEMENT

An analysis effort has been initiated to assess the detectability of decoupled explosions at regional distances as a function of source conditions, epicentral distance, frequency and background noise conditions. The investigation is focusing on a critical evaluation of the model described by Rodean of LLL at the recent ARPA Decoupling Conference. An attempt is being made to place reasonable upper and lower bounds on each of the elements which appear in this model in order to provide estimates on the range of the expected frequency dependent detectability at regional distances. For example, the source model used in Rodean's simulation is essentially the original Latter theoretical, low frequency approximation corresponding to a simple step in pressure acting on the cavity wall. Experience has shown that this provides a lower bound estimate on the amplitude of the decoupled source function (i.e., it predicts a decoupling factor of 200 for Sterling versus the inferred empirical value of about 70). The corresponding upper bound estimate for the source function has been obtained by reducing the Latter low frequency decoupling to match Sterling experience and modifying the high frequency spectral composition to include the effect of the initial pressure spike on the cavity wall. Similar lower and upper bounds are being defined for the controlling variables of the propagation path and local site noise conditions for use in a series of bounding detectability simulations.

3.2 GROUND MOTION ANALYSIS

Effort on this task has focused on the analysis of the free-field data from the Merlin event. The data recorded at

shot depth from this event over the distance range from about 200 to 750 m are unusual because of the presence of a late-time (i.e., greater than 1.2 seconds), relatively long-period ($\sim$ 0.8 second) secondary arrival. While this waveform is not particularly noticeable on accelerograms it is detectable on the velocity records and becomes quite prominent on the displacement records where amplitudes approach those of the direct arrivals. Three possible sources of this arrival have been considered: (1) free surface reflected phases (i.e., pP or pS), (2) reflections from a deep interface, and (3) spall closure.

First, with regard to surface reflected phases, the expected arrival times for pP (0.5 to 0.8 seconds) and pS (0.7 to 1.0 seconds) are significantly earlier than the observed arrival time of 1.3 to 1.7 seconds. Moreover, the observed radial displacement amplitudes associated with this arrival are nearly constant over the range 200 to 750 m, which is inconsistent with the behavior expected for pP or pS.

The second possibility considered was that the arrival represents a reflection from a deep interface. However, in order to explain the late arrival time, the interface would have to be located about 1 km below the shot and the apparent velocity across the shot depth stations from a reflection at this depth would be expected to be much greater than the observed apparent velocity of about 1800 m/sec. Moreover, the amplitude of a reflection from this depth would not be expected to be very large on the radial component.

Having eliminated surface reflections and deep reflections as explanations for the observation, we are left with spall closure. It is noted that the surface ground motion records from Merlin also show a relatively large arrival at late time (0.9 to 1.3 seconds) for stations with slant ranges from about 300 to 700 m. These signals coincide approximately with the arrival of what appears to be a rather prolonged spall

closure signal, although the observed period is substantially longer than that of the impulsive motion generally observed for spall closure at near stations. Calculations indicate that a P wave generated near the surface at the times and positions indicated by the surface recordings would arrive at the source-depth stations at about the same time as the unusual observed signals.

In fact, quantitative simulation of the spall closure as an axisymmetric distribution of vertical forces on the surface produces source depth pulses which agree remarkably well with the observations with regard to arrival time and amplitude/distance dependence. However, the sense of the predicted motion is out with respect to the explosive source as opposed to the observed inward displacement associated with the pulse in question. Near-field analytical solutions are currently being examined in an attempt to explain this puzzling phase problem.

IV. A FRACTURE CRITERION FOR FINITE DIFFERENCE MODELING OF EARTHQUAKE FAULTING

4.1 INTRODUCTION

In our previous three-dimensional simulations of earthquake faulting, we have modeled faulting as a propagating stress relaxation on a plane. We have bypassed much of the physics of the rupture process, however. Specifically, we have (1) prescribed the propagation of the fault surface, (2) constrained slip to be in a prescribed direction (parallel to the equilibrium shear stress in the fault plane), and (3) required the fault to heal permanently once the slip reversed direction.

We have developed a new algorithm governing three-dimensional frictional sliding which permits a more physical treatment of the fault, relaxing constraints 2 and 3. Changes in direction of sliding, as well as arrest and restarting of slip, are permitted during the faulting process. Arrest of sliding is determined, in the new algorithm, by fault dynamics, rather than being somewhat arbitrarily enforced when the sliding direction reverses. In fact, the notion of a velocity reversal, which is ill-defined when the slip direction is not specified a priori, is dispensed within the new algorithm.

The new frictional sliding algorithm is ideally suited for incorporating a fracture criterion, so that rupture advance is governed by rock strength rather than being arbitrarily prescribed (so that we can relax constraint 1). A physically acceptable fracture criterion should (a) dissipate energy at the crack tip and (b) lead to bounded stresses and velocities. A third requirement is motivated by numerical considerations; that is, an acceptable fracture criterion should be able to be formulated so as to be independent of zone-size, or nearly so.

The first two requirements are satisfied by the slip-weakening model investigated by Ida (1972) and Andrews (1976a). A two-dimensional numerical study by Andrews suggests that it is also zone-size independent. This model of failure presumes that the frictional traction, at a given point on the prospective fault plane, is a prescribed function of the total slip which has occurred at the point. This can be considered an idealization of a strain-weakening law.

In the next section we will outline the three-dimensional treatment of frictional sliding in the context of a simple Coulomb law. Then, the incorporation of a slip-weakening law requires only a minor refinement of the Coulomb law and is described in the subsequent section.

4.2 FINITE DIFFERENCE TREATMENT OF COULOMB FRICTION IN THREE-DIMENSIONAL CODES

A difficulty arises in three-dimensional numerical schemes when treating Coulomb frictional sliding on an interior surface, due to the fact that the sliding direction is, in general, not known a priori. A solution is presented here which resolves the difficulty. The method has been successfully incorporated into the TRES three-dimensional finite difference code.

Physically, the frictional traction on a slip surface is required to contribute an acceleration in the direction opposed to the instantaneous slip velocity. However, in numerical time-stepping schemes, velocity and acceleration are centered differently in time. This is not a trivial discrepancy; if the direction of the frictional acceleration contribution at time t is determined from the velocity at time $t - \Delta t/2$ (where Δt is the time increment), friction will generally have a component in the direction of sliding. Even if this component is initially small, it will add energy to

the system, and the resulting behavior is unstable. A related difficulty is that since the slip has two components, it becomes impossible to detect a slip velocity zero, since velocity is known only at discrete times. Thus, it is not obvious how to formulate a criterion for the arrest of slip at a point.

We assume that slip is confined to the plane $z = 0$, and is governed by a Coulomb law. $\underline{s}(t)$ denotes the slip vector (+z side relative to -z side) at time t at a point in the plane $z = 0$. Only tangential slip is permitted. $\underline{\tau}$ denotes the tangential traction exerted on the +z halfspace at $z = 0$. $\underline{\tau}_c$ is the value of this tangential traction required to enforce continuity of velocity, and σ_f is the magnitude of the sliding frictional stress (σ_f is positive and proportional to the compressive stress, $-\sigma_{zz}$, on the slip plane). With these definitions, the friction law takes the form of the following boundary condition on $z = 0$:

$$\underline{\tau} = \begin{cases} -\sigma_f \dfrac{\dot{\underline{s}}}{|\dot{\underline{s}}|} & \text{if } |\underline{\tau}_c| \geq \sigma_f \\ \underline{\tau}_c & \text{if } |\underline{\tau}_c| < \sigma_f \end{cases} . \qquad (1)$$

We write the x and y components of displacement $\underline{u}$ at the slip plane $z = 0$, as the sum of a continuous part (q) and a discontinuity (s):

$$u_x = q_x + s_x$$

$$u_y = q_y + s_y$$

(u_z is continuous). Assuming an explicit difference scheme, the $\dot{q}$'s and $\dot{s}$'s are determined at times $(n-1/2)\Delta t$ (Δt is the time step, n is an integer) and the s's and q's at times $n\Delta t$ by recursion relations of the form

$$\dot{s}_x^n = \dot{s}_x^{n-1} + \Delta t \left[F_x\left(s_x^{n-1}, s_y^{n-1}, q_x^{n-1}, q_y^{n-1}, u_z^{n-1}\right) + T_x \right] \quad \text{(a)}$$

$$\dot{s}_y^n = \dot{s}_y^{n-1} + \Delta t \left[F_y\left(s_x^{n-1}, s_y^{n-1}, q_x^{n-1}, q_y^{n-1}, u_z^{n-1}\right) + T_y \right] \quad \text{(b)}$$

$$\dot{q}_x^n = \dot{q}_x^{n-1} + \Delta t\, G_x\left(s_x^{n-1}, s_y^{n-1}, q_x^{n-1}, q_y^{n-1}, u_z^{n-1}\right) \quad \text{(c)}$$

$$\dot{q}_y^n = \dot{q}_y^{n-1} + \Delta t\, G_y\left(s_x^{n-1}, s_y^{n-1}, q_x^{n-1}, q_y^{n-1}, u_z^{n-1}\right) \quad \text{(d)}$$

$$\dot{u}_z^n = \dot{u}_z^{n-1} + \Delta t\, G_z\left(s_x^{n-1}, s_y^{n-1}, q_x^{n-1}, q_y^{n-1}, u_z^{n-1}\right) \quad \text{(e)}$$

$$s_x^n = s_x^{n-1} + \Delta t\, \dot{s}_x^n \quad \text{(f)}$$

$$s_y^n = s_y^{n-1} + \Delta t\, \dot{s}_y^n \quad \text{(g)}$$

$$q_x^n = q_x^{n-1} + \Delta t\, \dot{q}_x^n \quad \text{(h)}$$

$$q_y^n = q_y^{n-1} + \Delta t\, \dot{q}_y^n \quad \text{(i)}$$

$$u_z^n = u_z^{n-1} + \Delta t\, \dot{u}_z^n \quad . \quad \text{(j)}$$

(2)

F_x, F_y, G_x, G_y, and G_z are spatial difference operators, the G's representing continuous accelerations, the F's a discontinuity in acceleration.

T_x and T_y represent the acceleration due to the boundary stresses from Equation (1). The most obvious form for T_x and T_y would be

$$\left.\begin{aligned} T_x &= -A\sigma_f \frac{\dot{s}_x^{n-1}}{\left[\left(\dot{s}_x^{n-1}\right)^2 + \left(\dot{s}_y^{n-1}\right)^2\right]^{1/2}} \\ T_y &= -A\sigma_f \frac{\dot{s}_y^{n-1}}{\left[\left(\dot{s}_x^{n-1}\right)^2 + \left(\dot{s}_y^{n-1}\right)^2\right]^{1/2}} \end{aligned}\right\} \text{ if } T_c \geq \sigma_f \qquad (3a)$$

$$\left.\begin{aligned} T_x &= -\frac{\dot{s}_x^{n-1}}{\Delta t} - F_x \\ T_y &= -\frac{\dot{s}_x^{n-1}}{\Delta t} - F_y \end{aligned}\right\} \text{ if } T_c < \sigma_f \qquad (3b)$$

where

$$T_c \equiv \frac{1}{A}\left[\left(\frac{\dot{s}_x^{n-1}}{\Delta t} + F_x\right)^2 + \left(\frac{\dot{s}_y^{n-1}}{\Delta t} + F_y\right)^2\right]^{1/2} \qquad (4)$$

(A is positive constant, involving density and spatial zone size, which converts stress to nodal acceleration).

Unfortunately, Equation (3), combined with Equations (2a) and (2b), leads to an instability, due to the fact that the T's are centered (1/2)Δt earlier in time than the F's. A solution proposed by Day (1977) has been found to provide a stable solution. Centering is modified by replacing Equation (3) with an average over two time steps:

$$
\left.
\begin{aligned}
T_x &= -\frac{A\sigma_f}{2}\left\{\frac{\dot{s}_x^{n-1}}{\left[\left(\dot{s}_x^{n-1}\right)^2+\left(\dot{s}_y^{n-1}\right)^2\right]^{1/2}}+\frac{\dot{s}_x^{n}}{\left[\left(\dot{s}_x^{n}\right)^2+\left(\dot{s}_y^{n}\right)^2\right]^{1/2}}\right\} \\
T_y &= -\frac{A\sigma_f}{2}\left\{\frac{\dot{s}_y^{n-1}}{\left[\left(\dot{s}_x^{n-1}\right)^2+\left(\dot{s}_y^{n-1}\right)^2\right]^{1/2}}+\frac{\dot{s}_y^{n}}{\left[\left(\dot{s}_x^{n}\right)^2+\left(\dot{s}_y^{n}\right)^2\right]^{1/2}}\right\}
\end{aligned}
\right\} \text{ if } T_c \geq \sigma_f \qquad (5)
$$

$$
\left.
\begin{aligned}
T_x &= -\frac{\dot{s}_x^{n-1}}{\Delta t} - F_x \\
T_t &= -\frac{\dot{s}_y^{n-1}}{\Delta t} - F_y
\end{aligned}
\right\} \text{ if } T_c < \sigma_f \quad .
$$

However, a new definition of T_c associated with Equation (5) is necessary, and will be derived below.

Inserting Equation (5) into 2a and 2b leads to a pair of coupled nonlinear equations for unknowns $\dot{s}_x^n$ and $\dot{s}_y^n$:

$$\dot{s}_x^n = C_x - \frac{B\,\dot{s}_x^n}{\left[\left(\dot{s}_x^n\right)^2 + \left(\dot{s}_y^n\right)^2\right]^{1/2}}$$

$$\dot{s}_y^n = C_y - \frac{B\,\dot{s}_y^n}{\left[\left(\dot{s}_x^n\right)^2 + \left(\dot{s}_y^n\right)^2\right]^{1/2}} \qquad (6)$$

where

$$C_x = \dot{s}_x^{n-1} + \Delta t F_x - \frac{\Delta t A \sigma_f}{2} \frac{\dot{s}_x^{n-1}}{\left[\left(\dot{s}_x^{n-1}\right)^2 + \left(\dot{s}_y^{n-1}\right)^2\right]^{1/2}}$$

$$C_y = \dot{s}_y^{n-1} + \Delta t F_y - \frac{\Delta t A \sigma_f}{2} \frac{\dot{s}_y^{n-1}}{\left[\left(\dot{s}_x^{n-1}\right)^2 + \left(\dot{s}_y^{n-1}\right)^2\right]^{1/2}}$$

and

$$B = \frac{\Delta t A \sigma_f}{2} \quad .$$

These have the solution (see Day, 1977)

$$\left.\begin{aligned} \dot{s}_x^n &= C_x - \frac{B\,C_x}{\left(C_x^2 + C_y^2\right)^{1/2}} \\ \dot{s}_y^n &= C_y - \frac{B\,C_y}{\left(C_x^2 + C_y^2\right)^{1/2}} \end{aligned}\right\} \text{ if } \left(C_1^2 + C_2^2\right)^{1/2} \geq B \quad ,$$

which provides a stable scheme for updating $\dot{s}_x$ and $\dot{s}_y$. If $\left(C_1^2 + C_2^2\right)^{1/2} < B$, no solution exists for Equation (6), which suggests that we redefine T_c as

$$T_c \equiv \frac{2}{A}\left\{\left[\frac{\dot{s}_x^{n-1}}{\Delta t} + F_x - \frac{\sigma_{fA}}{2}\frac{\dot{s}_x^{n-1}}{\left[\left(\dot{s}_x^{n-1}\right)^2 + \left(\dot{s}_y^{n-1}\right)^2\right]^{1/2}}\right]^2 + \left[\frac{\dot{s}_y^{n-1}}{\Delta t} + F_x - \frac{\sigma_{fA}}{2}\frac{\dot{s}_y^{n-1}}{\left[\left(\dot{s}_x^{n-1}\right)^2 + \left(\dot{s}_y^{n-1}\right)^2\right]^{1/2}}\right]^2\right\}^{1/2} \tag{7}$$

and replace Equation (2a), (2b), (3a), and (3b) with

$$\begin{aligned} \dot{s}_x^n &= C_x\left[1 - \frac{B}{\left(C_x^2 + C_y^2\right)^{1/2}}\right] \\ \dot{s}_y^n &= C_y\left[1 - \frac{B}{\left(C_x^2 + C_y^2\right)^{1/2}}\right] \end{aligned} \qquad \text{if } T_c \geq \sigma_f \tag{8}$$

$$\begin{aligned} \dot{s}_x^n &= 0 \\ \dot{s}_y^n &= 0 \end{aligned} \qquad \text{if } T_c < \sigma_f \quad .$$

Equation (8) provides well-behaved simulation of Coulomb friction. The condition $T_c < \sigma_f$, with T_c given by Equation (7), is the criterion for arrest of sliding. Mathematically, this condition says that the velocity must be continuous when no solution exists to the system (6). Physically, it says that slip must be arrested at time $n\Delta t$ if a slip velocity zero will occur due to frictional deceleration during the

subsequent $(1/2)\Delta t$. If the slip velocity were not set to zero, the frictional force would be acting to accelerate slip during part of that $(1/2)\Delta t$.

The TRES finite difference code (Cherry, 1977) has previously avoided the problem by artificially constraining slip to occur in a prescribed direction only. Equation (8) has been incorporated into TRES, permitting this constraint to be relaxed. The algorithm governing frictional sliding in TRES has actually been considerably simplified as a result.

4.3 SLIP-WEAKENING CONSTITUTIVE MODEL

Ida (1972) investigated the two-dimensional, anti-plane-strain dynamics of a slip-weakening failure model. In this model, a finite shear strength, $\sigma_0(0)$, is assigned to the fault prior to initiation of sliding. Slip commences at a point when necessary to prevent a stress concentration in excess of $\sigma_0(0)$. The relative displacement, with amplitude denoted by s, is assumed to weaken the fault plane at that point according to some prescribed function $\sigma_0(s)$ until the fault loses all cohesion and reaches the kinetic friction level, $\sigma_0(D)$, where D is the slip required to eliminate cohesion. The amount of energy required per unit area to destroy cohesion, denoted 2G, is

$$2G = \int_0^D [\sigma_0(s) - \sigma_0(D)]\, ds \ . \tag{9}$$

A simple slip-weakening law can be immediately introduced in Equation (8). All that is necessary is that σ_f in Equation (8) be made a function of the slip:

$$\sigma_f = \begin{cases} \sigma_0(s), & \text{if } s < D \\ \\ \sigma_0(D), & \text{if } s \geq 0 \end{cases} , \tag{10}$$

where D is a specified constant, and the function $\sigma_0(s)$ is a prescribed function for $0 \leq s \leq D$. Ida's analysis suggests that if σ_0 is assumed to be fairly smooth, the behavior of the slip function is insensitive to the precise shape of σ_0. Currently, we prescribe σ_0 to be linear.

An algorithm based on Equation (8), with σ_f determined as in Equation (10), has been communicated to the Institute for Advanced Computation (IAC) programmers. They are in the process of incorporating the model into I4TRES, the ILLIAC IV version of TRES. When the ILLIAC program modifications are completed, we will begin examining the role of the surface energy, G, in determining the shape and rate of advance of the rupture. Of particular interest initially will be whether rupture velocities exceeding the S wave speed develop for three-dimensional rupture models, as they persistently do for two-dimensional numerical models (Andrews, 1976b; Das and Aki, 1977). Subsequently, we will look at the role of stress heterogeneities in stopping the rupture.

This constitutive model can be viewed as an idealization of a strain-weakening constitutive law. Andrews (1976a) has argued that G cannot be considered a material constant, at least once the fault has grown beyond a certain limiting size. Eventually, inelastic dissipation is expected to involve a widening zone about the fault plane. At this point the slip-weakening idealization becomes inadequate, unless G is increased to properly account for the increasing inelastic work. Our approach is to analyze the simple slip-weakening model, recognizing its probable limitations, and then generalize it to include realistic inelastic behavior off the fault plane.

V. SOURCE CALCULATIONS

An extensive one- and two-dimensional effort is continuing to simulate the ground motion from the PILEDRIVER event in NTS fractured granodiorite. Of particular interest are the effects of the free surface (spall, overburden, etc.) on the far-field ground motion. The two-dimensional calculations to be believable should be in agreement with the measured free-field and free surface velocity data (Perret, 1968; Hoffman and Sauer, 1969). It is well known that these data cannot be matched using the triaxial failure envelope measured in the laboratory either for competent or fractured granite. We have reported earlier (Bache, et al., 1978) the results of one-dimensional free field calculations made using an effective stress model which accounts for the water present in the jointed granite. These calculations were in excellent agreement with the measured cavity radius and in fairly good agreement with the velocity data from two shot level stations reported by Perret. However, a preliminary two-dimensional calculation made with the same material properties did not give a good match to the rest of the free-field data or to the free surface data. A longer duration of the positive velocity pulse was required to better match the free field data.

A series of one-dimensional free field calculations has been made to investigate the effect of changes at the low pressure end of the failure surface (the higher pressure failure envelope for fractured granite is well defined). For a given choice of Y_o, the strength at $\bar{P} = 0$ (see Bache, et al., 1978 for details of the shear failure model), we attempted to match the calculation to the free field data through a judicious choice of P_c, the pressure at which all air-filled pores are closed. Our strength model directly links the air-filled porosity to the effective pressure, the difference between the pressure in the rock and the pressure in the pore water. When

P_c is reached, the rock is considered to be in pressure equilibrium so that the effective pressure is zero. Since the shear strength of the rock is a function of the effective stress, a high value of P_c means that a smaller region sees the lower strength. We believe that P_c cannot be more than a few kilobars as most of the porosity for the granodiorite is considered to be in the form of easily closed cracks.

The velocity gauge data at the two Perret shot level stations were successfully matched in two free field calculations. Figures 4 and 5 show the agreement between the data and Calculation 1 made with a relatively low strength Y_o = 20 bars and with P_c = 2.0 kb. Figures 6 and 7 show comparisons between the data and Calculation 2 for Y_o = 100 bars and P_c = 1.0 kb. There appears to be little to choose between the two calculations based on the velocity data or even based on the transform of the reduced velocity potential (RVP). (Calculation 1 has a slightly lower corner frequency but a larger static RDP.) However, the different values of Y_o should strongly influence the yielding and spall near the free surface. A choice may be made based on the calculated cavity radii; 47.4 meters for Calculation 1 versus 39.5 meters for Calculation 2. The more widely accepted measurements of cavity radius are 40 meters, based on drillback into the lower half of the PILEDRIVER cavity, and 44.5 meters calculated from the void volume of the chimney determined from chimney pressurization tests. (The latter number is in better agreement with the scaled cavity radius from HARDHAT, a nuclear event in the same material as PILEDRIVER.) A final determination on which calculation to accept has not been made at this time and will, of course, depend upon the results of two-dimensional studies.

Several additional coarsely zoned two-dimensional calculations have been made, each one incorporating more of the geologic structure of the PILEDRIVER site. Calculation PD15 used the time of arrival data as reported by Hoffman and Sauer

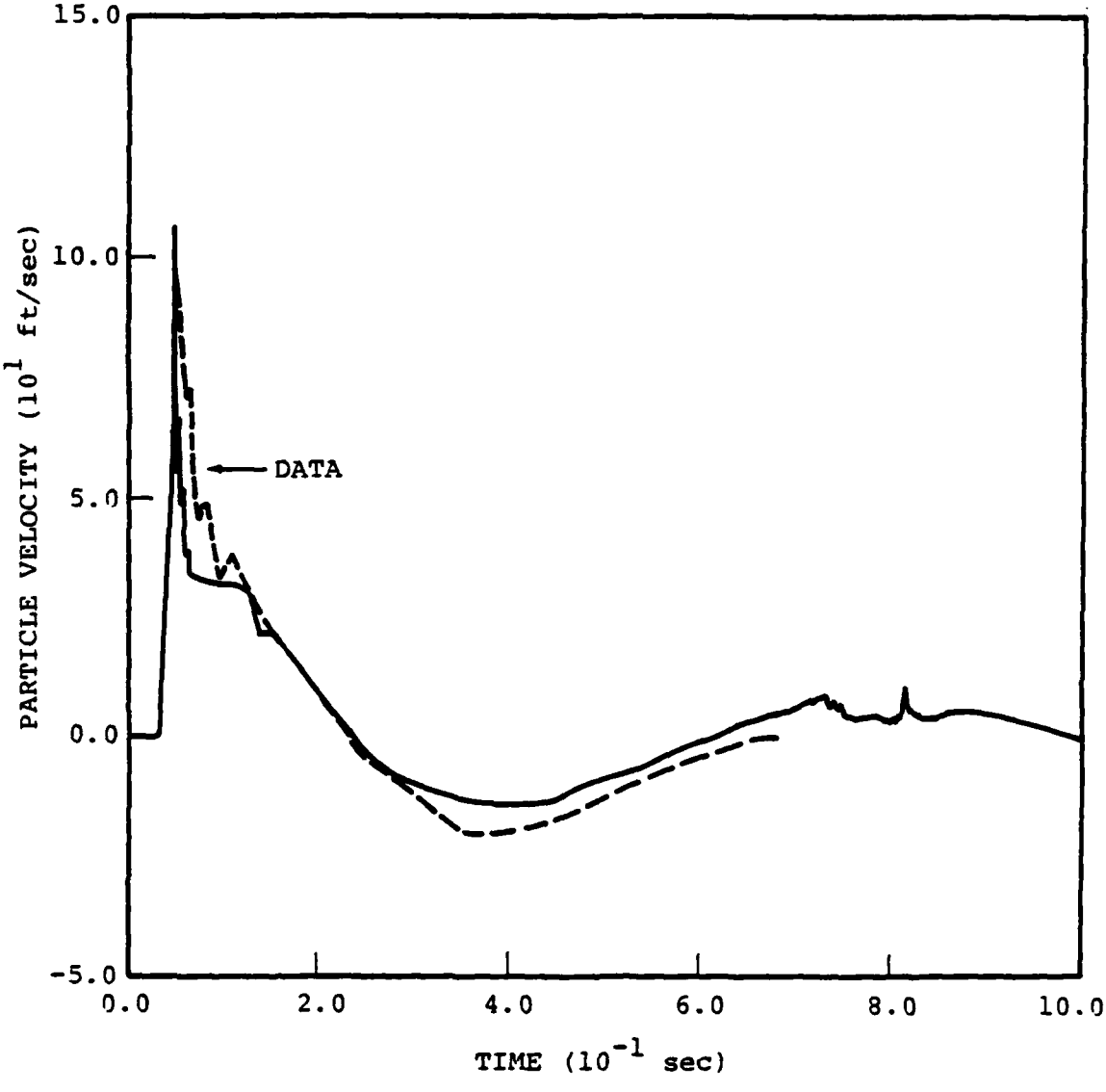

Figure 4. Comparison between data and Calculation 1 (P_c = 2.0 kb, Y_o = 20 bars) at first Perret station (668 feet from WP).

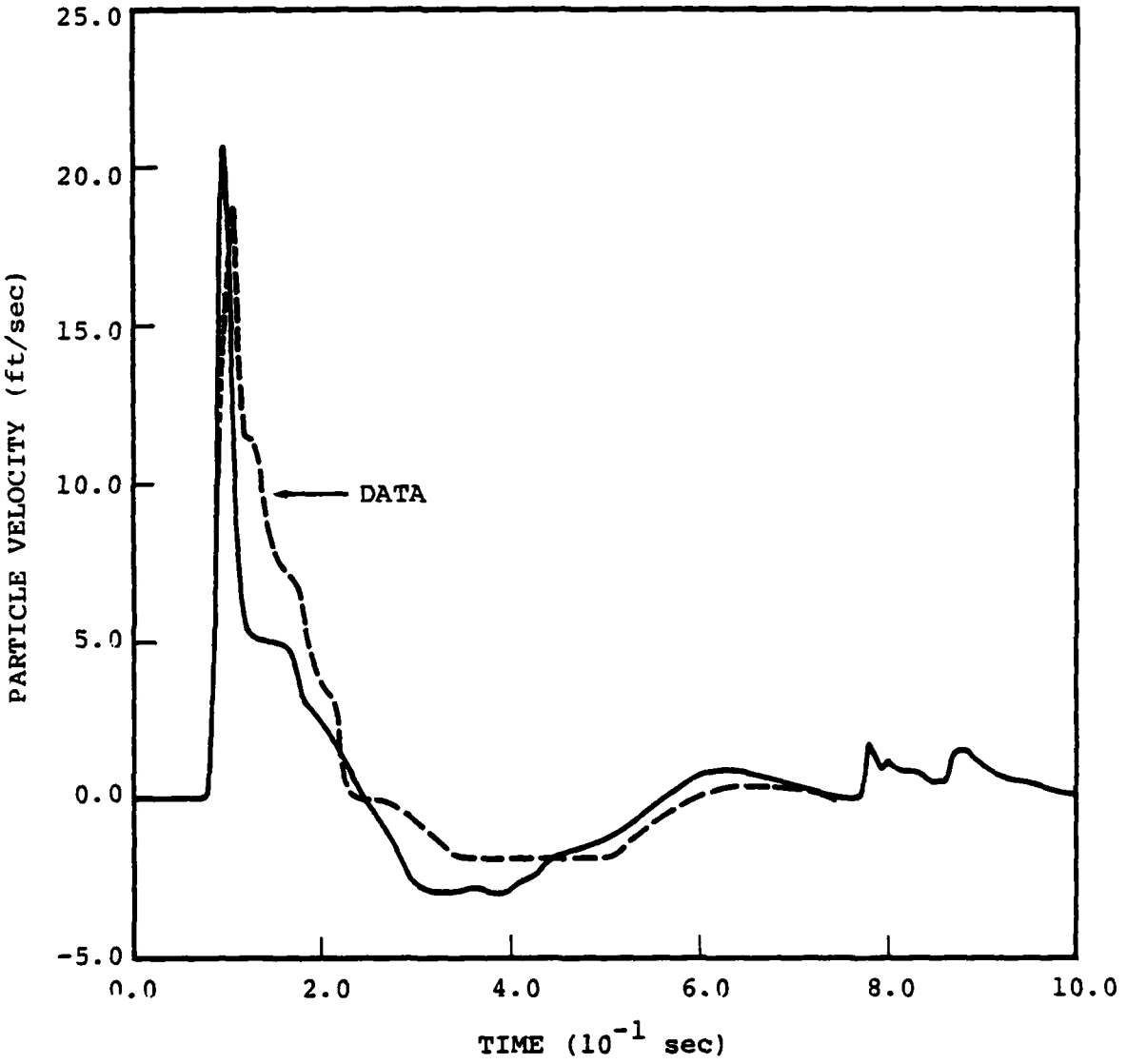

Figure 5. Comparison between data and Calculation 1 (P_c = 2.0 kb, Y_o = 20 bars) at second Perret station (1543 feet from WP).

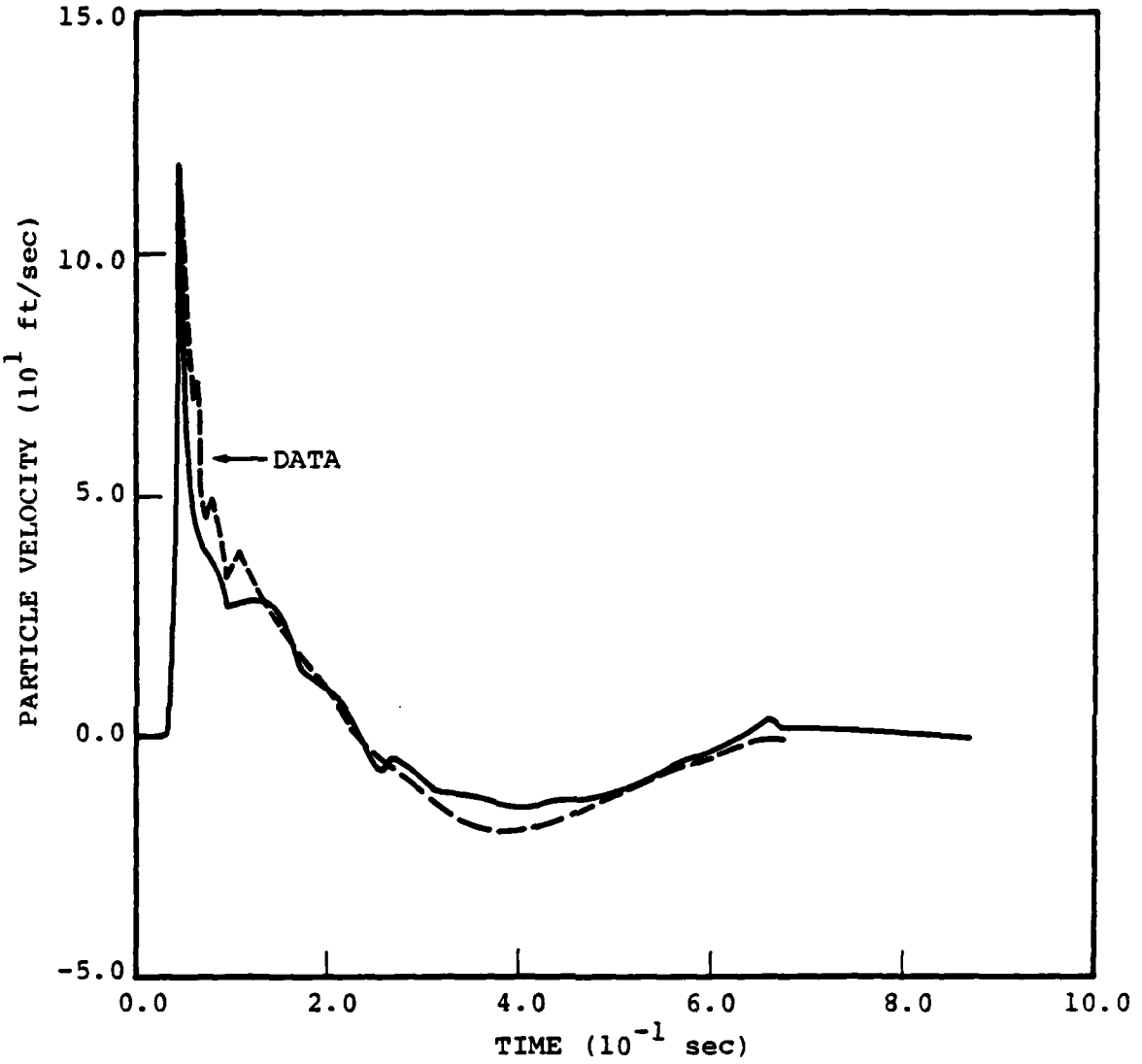

Figure 6. Comparison between data and Calculation 2 (P_C = 1.0 kb, Y_O = 100 bars) at first Perret station.

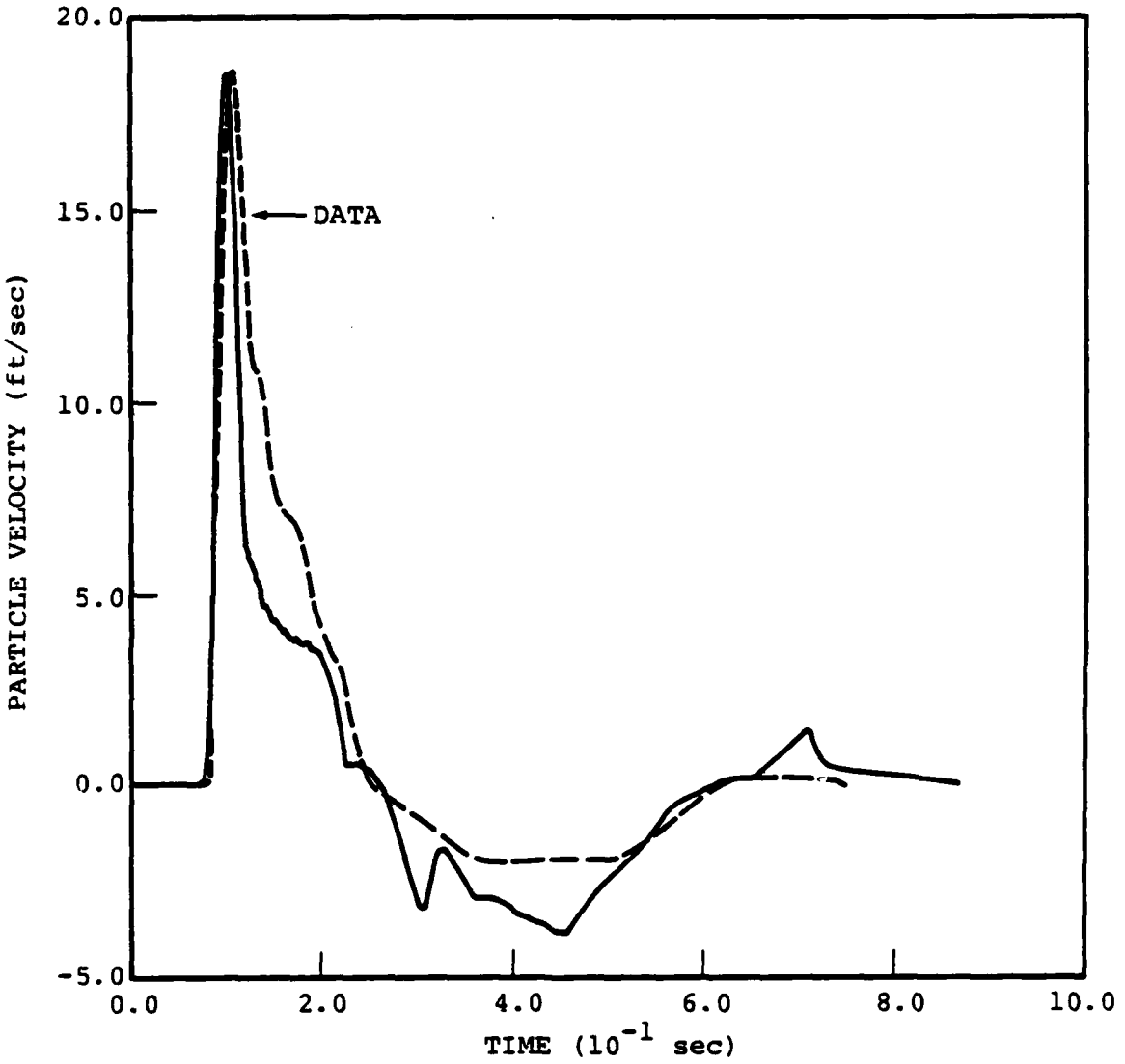

Figure 7. Comparison between data and Calculation 2 (P_c = 1.0 kb, Y_o = 100 bars) at second Pefret station.

to locate two horizontal layers approximately 350 and 420 meters above the working point. This calculation used the material properties of Calculation 1 for the working point layer of material.

Another two-dimensional calculation (PD16) used the material properties of Calculation 2 for the working point material and the time of arrival data to define the other two layers as before. Calculation PD16 also assumed that the boundary between the working point layer and the layer above it was the location of the water table as well. The effective stress law was only used below the water table.

Calculation PD16 has been the most encouraging calculation made to this date, giving good agreement with much of the data. However, the coarse zoning in this preliminary calculation has not allowed us to model with sufficient accuracy the spall at the free surface. Future calculations will locate the water table more accurately and attempt to model the spall in greater detail.

A parallel effort, using one-dimensional calculations, is underway to model the French nuclear tests in the granite of the Hoggar Massif in the Sahara Desert. Laboratory tests on core samples have indicated that the strength and other material properties of this rock are fairly similar to NTS granodiorite. Of course, the Hoggar rock is very dry. To first approximation (material properties are not identical), calculations in Hoggar granite may then be made with the same material properties as for PILEDRIVER, but excluding the effective stress law. Analogous calculations to PILEDRIVER Calculations 1 and 2 have been made for Hoggar without the effective stress model. These calculations show considerably smaller cube root scaled cavity radii than PILEDRIVER, but are within three percent and nine percent, respectively, of the cavity radii reported by the French. The RVP transforms computed

from the Hoggar calculations show relatively little peaking of the spectra. The static RDP is approximately a factor of three to five lower than computed for PILEDRIVER.

In summary, partial saturation coupled with an effective stress law provides a constitutive model which gives an acceptable fit to the PILEDRIVER free field ground motion data and the measured cavity radius. A match to the reported Hoggar cavity radii is obtained by assuming strengh characteristics appropriate for a dry rock environment. The resulting seismic coupling is a factor of three to five greater for the PILEDRIVER environment than for Hoggar. If we believe the reported Hoggar cavities, then for identical propagation path characteristics, a given yield in the PILEDRIVER environment would generate teleseismic body waves which would be three to five times larger than those produced by the same yield in the Hoggar environment.

VI. DECOUPLING CALCULATIONS IN SALT

Figure 8 shows the amplitude spectra of the reduced velocity potential (RVP) for SALMON free field data (Springer, et al., 1968). We have calculated RVP spectra for 0.38 kt (the STERLING yield) detonated in a 18 meter cavity.

Two calculations were completed for this cavity radius, one involving detonation in a mined cavity and the other detonation in a cavity with the rock outside the cavity weakened from shock heating. The amount of thermal weakening was estimated from a calculation of the SALMON event.

Figure 9 shows the decoupling ratios between the RVP spectra shown in Figure 8 (scaled to 0.38 kt) and these two calculations. For frequencies less than 7 Hz the decoupling ratio is approximately 130 for the mined cavity and 110 for the thermally weakened SALMON cavity. Figure 10 shows the decoupling ratio between the RVP spectrum in Figure 8 and the spectrum from 5.3 kt detonated in a 50 meter mined cavity. The decoupling ratio is approximately 130 but the corner frequency has decreased to 2.5 Hz due to detonation in the larger cavity.

Near Source Attenuation

Figure 11 shows a comparison between calculated and observed peak radial stress and particle velocity from the SALMON event. The elastic radius from the calculation occurs at approximately 300 meters while the data shows no apparent change of slope over the entire distance range.

A possible explanation for this discrepancy is that the peak particle velocity (and stress) is sensitive to the high frequency components of the seismic source while the nonlinear constitutive models for fracture, plastic flow,

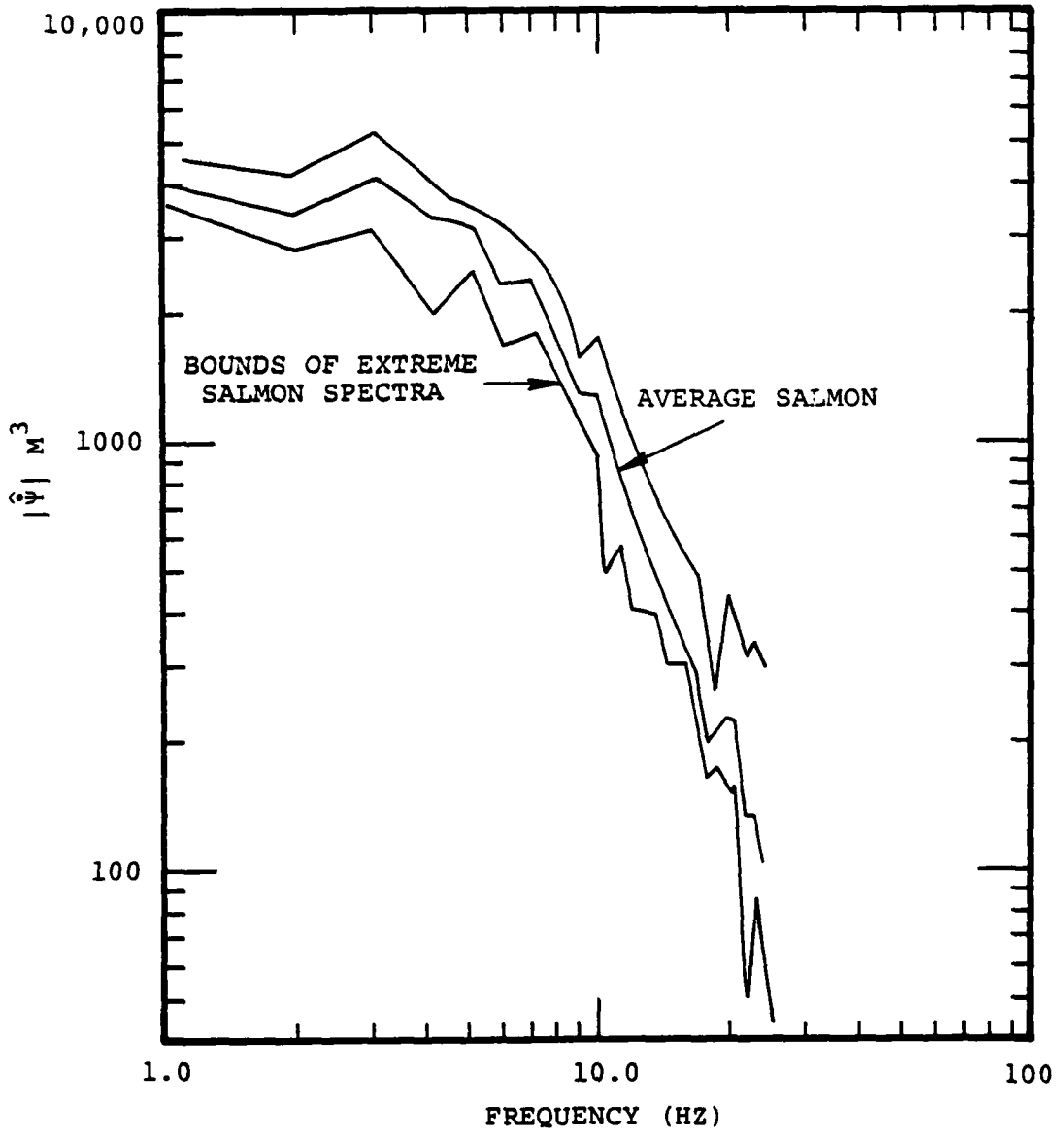

Figure 8. Amplitude spectrum of the SALMON reduced velocity potential (Springer, et al., 1968).

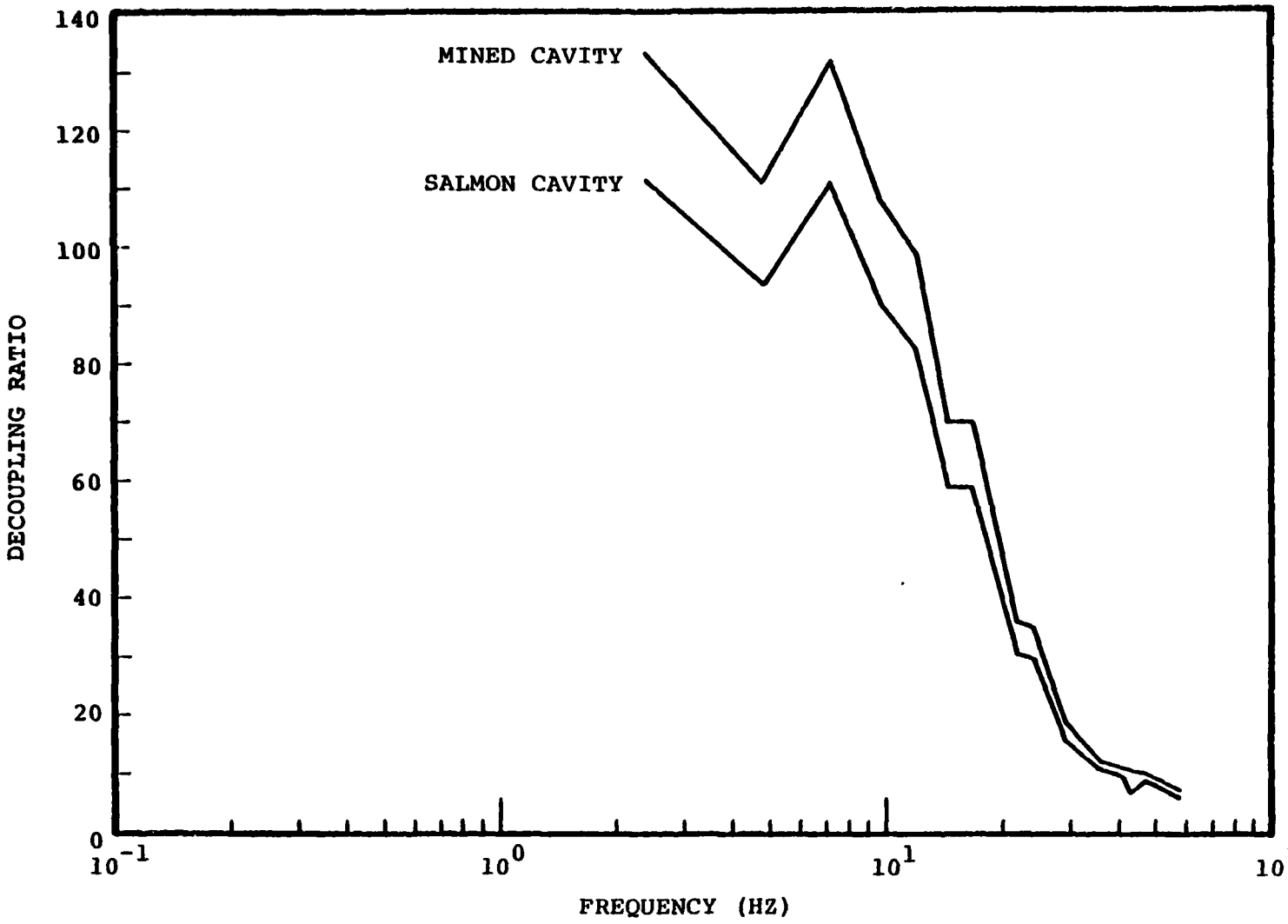

Figure 9. Decoupling ratio between SALMON data, Figure 8, scaled to 0.38 kt, and two calculations for 0.38 kt detonated in a 18 meter cavity.

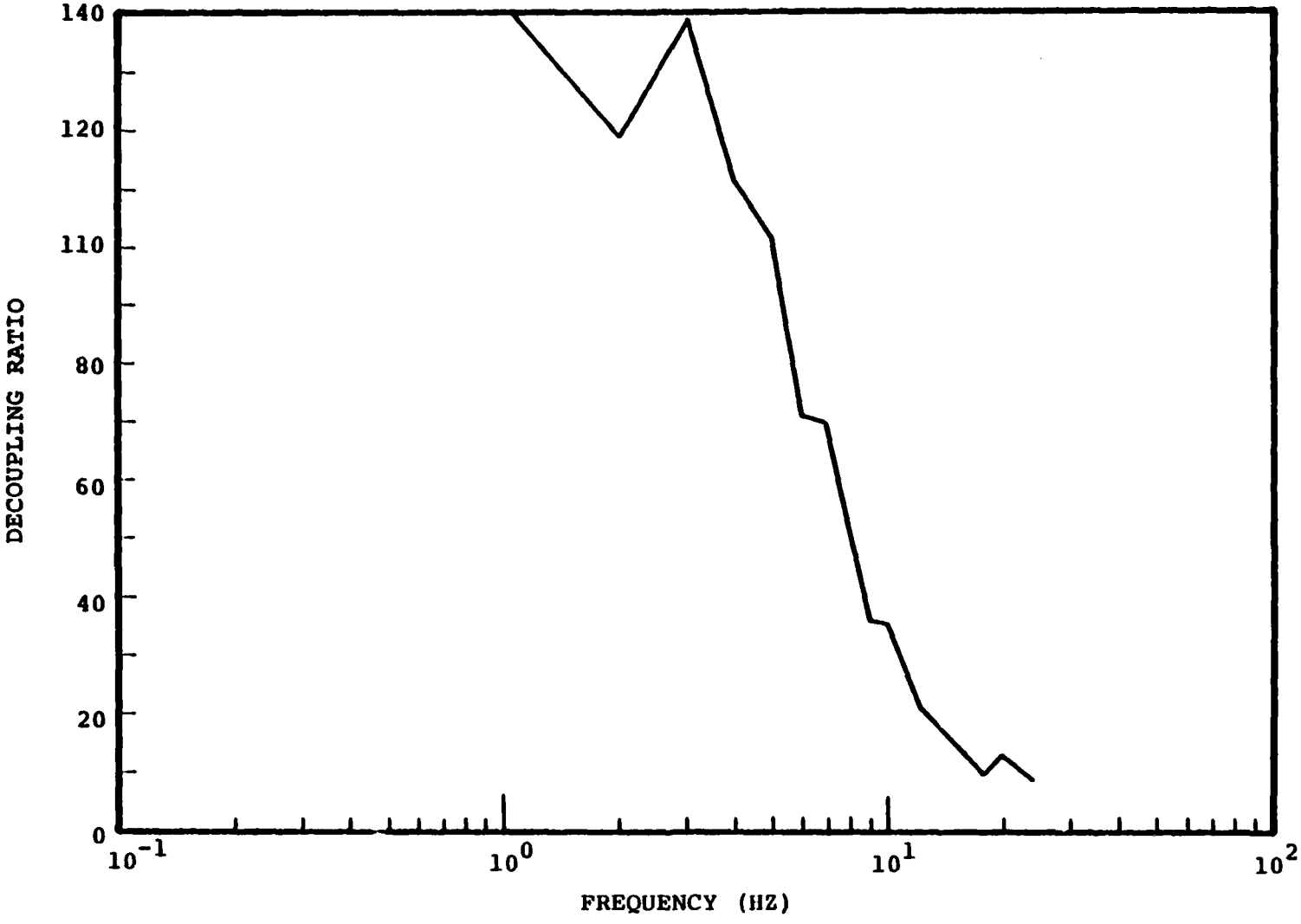

Figure 10. Decoupling ratio between SALMON data, Figure 8, and 5.3 kt detonated in a 50 meter mined cavity.

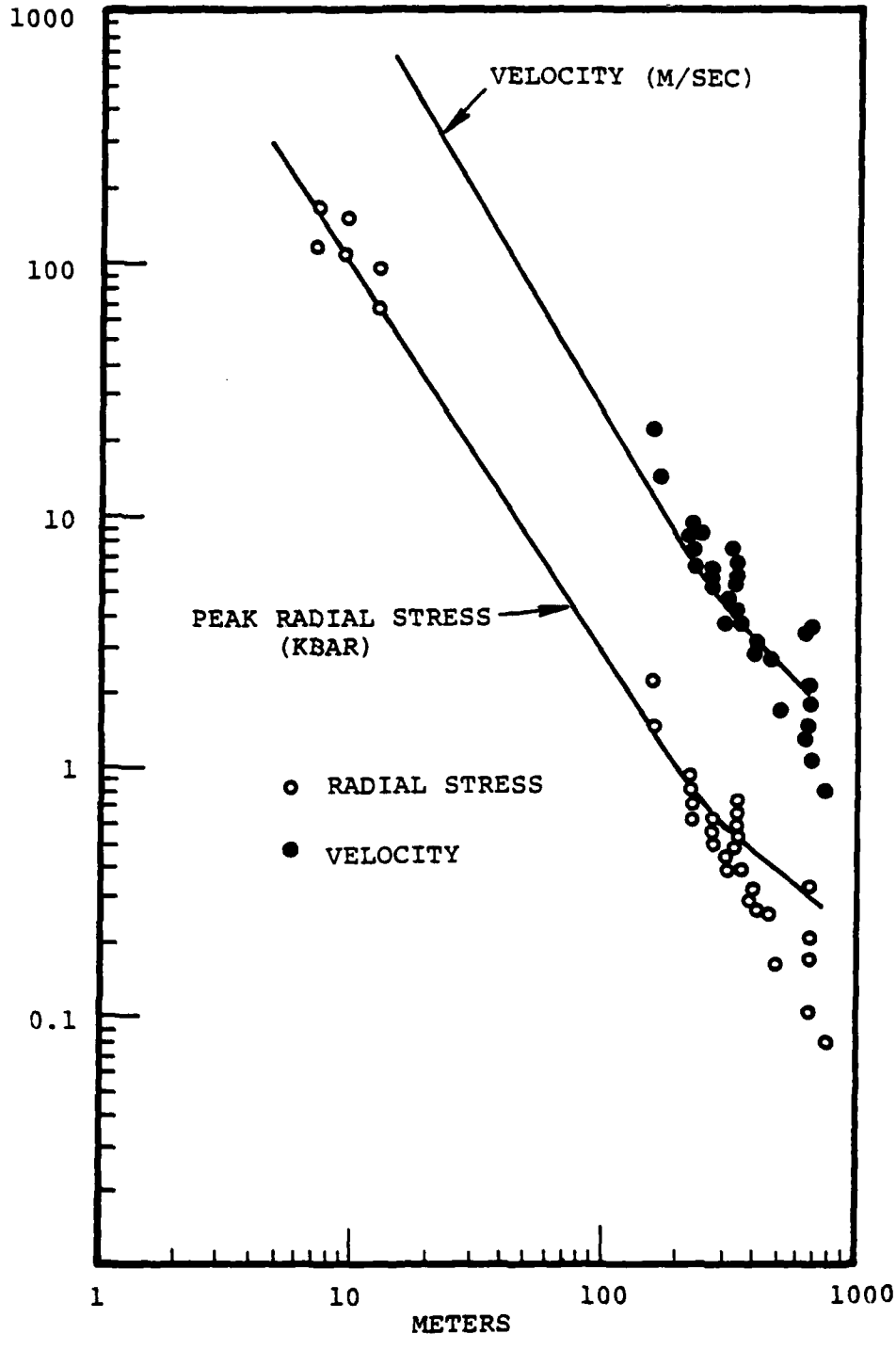

Figure 11. Calculated and experimental peak velocity and peak radial stress as a function of radius in horizontal direction from the shot point.

irreversible pore collapse and effective stress are not intended to model the anelastic attenuation of small deformation elastic waves.

In order to quantify this hypothesis we have investigated the effect of Q on peak displacement, particle velocity and radial stress.

Figure 12 shows the change in the calculated RVP spectrum for SALMON over the distance range 0.3 km < R < 0.6 km due to convolution with the attenuation operator.

$$e^{-\frac{\pi f(R - 0.3\ \text{km})}{\alpha Q}}$$

where Q = 10. The change in the spectrum for frequencies less than 10 Hz is not dramatic even with attenuation this severe.

Figure 13 shows the effect of Q on peak displacement, particle velocity and stress. We see a large change in the attenuation rate for peak velocity and stress when Q changes from infinity to ten. This is a lesser change in the attenuation of peak displacement, almost certainly caused by the lower frequencies responsible for this quantity.

It seems that most of the problems associated with the observed attenuation rate of peak velocity, stress and displacement versus those predicted by nonlinear finite difference codes can be resolved by the addition of anelastic attenuation to the equivalent source predicted by the codes. This has been our approach from the beginning. In addition, measurements of the peaks can be used to infer the Q appropriate for propagation of this source to distances beyond the elastic radius.

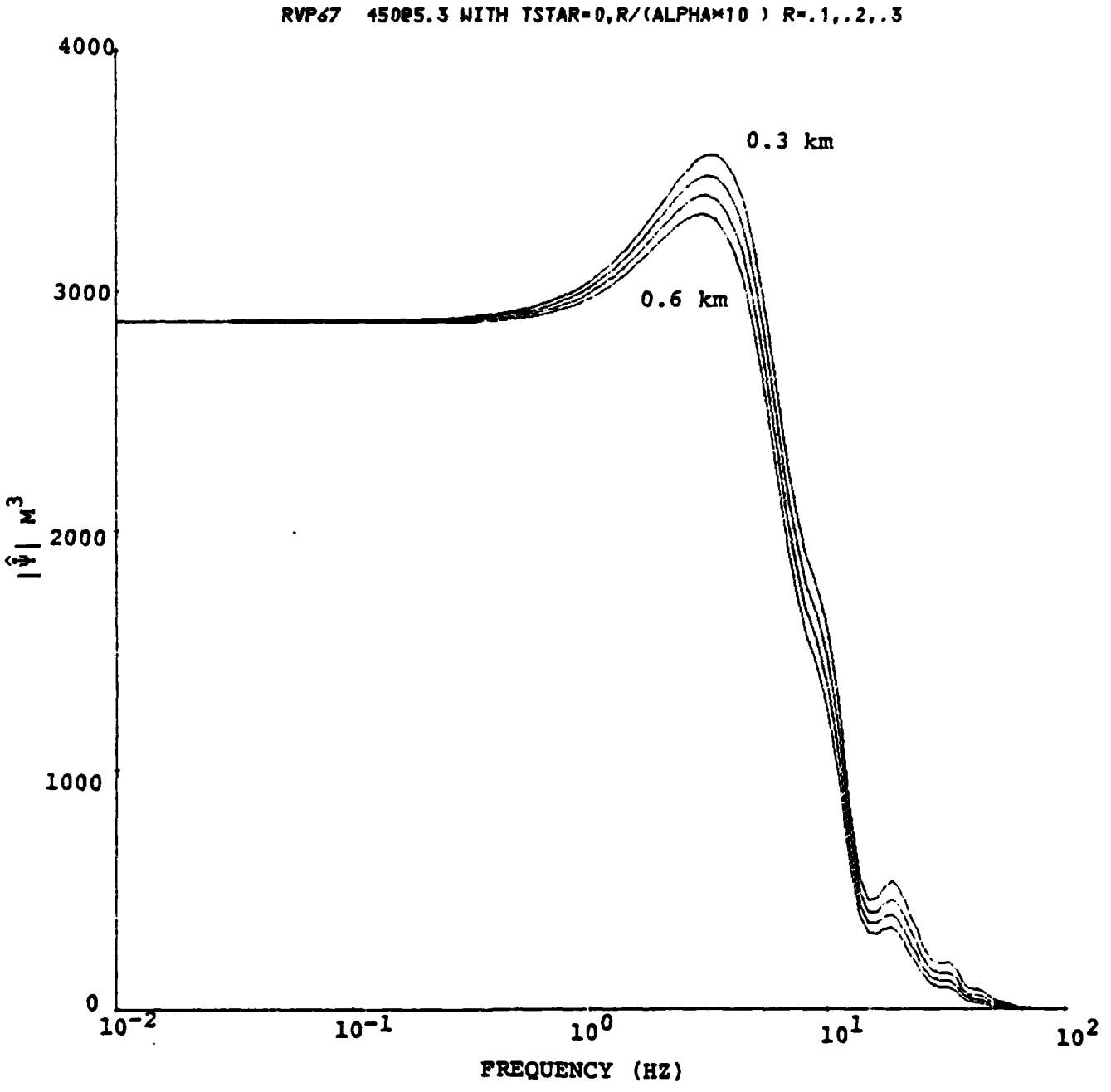

Figure 12. The effect of Q = 10 on the RVP spectra.

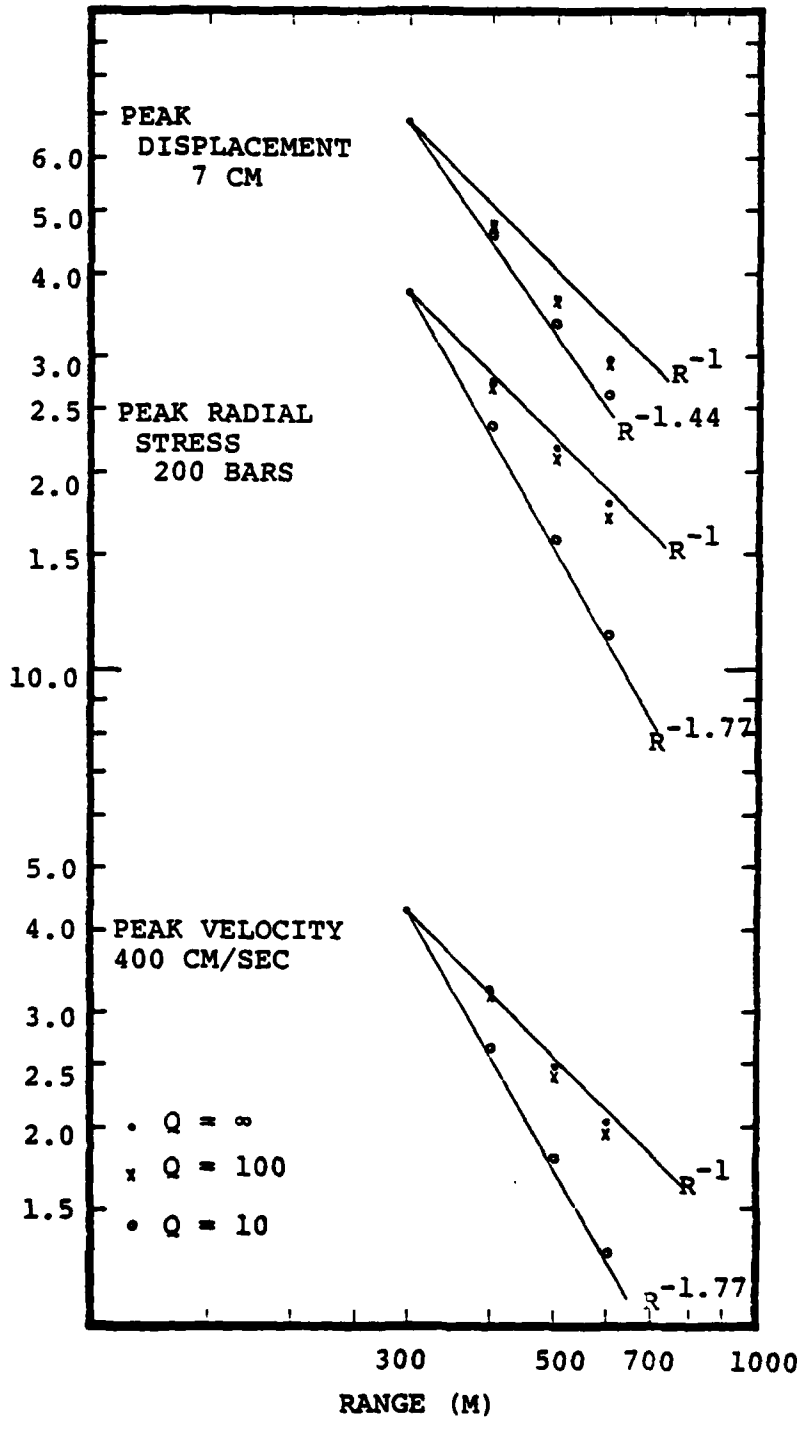

Figure 13. The effect of Q on peak displacement, stress and velocity.

REFERENCES

Andrews, D. J. (1976a), "Rupture Propagation with Finite Stress in Antiplane Strain," J. Geophys. Res., 81, pp. 3575.

Andrews, D. J. (1976b), "Rupture Velocity of Plane Strain Shear Cracks," J. Geophys. Res., 81, pp. 5679.

Bache, T. C., J. M. Savino, S. M. Day, J. T. Cherry, H. J. Swanger and N. Rimer (1978), "Summary of Seismic Discrimination and Explosion Yield Determination Research," Systems, Science and Software Final Report submitted to the Advanced Research Projects Agency, SSS-R-79-3847, November.

Cherry, J. T. (1977), "Users' Manual for the TRES Code," Systems, Science and Software Report SSS-R-77-3128, January.

Das, S. and K. Aki (1977), "A Numerical Study of Two-Dimensional Spontaneous Rupture Propagation," Geophys. J. R. Astr. Soc., Vol. 50, pp. 643-668.

Day, S. M. (1977), "Finite Element Analysis of Seismic Scattering Problems," Ph.D. Dissertation, University of California, San Diego.

Day, S. M., T. C. Bache, T. G. Barker and J. T. Cherry (1978) "A Source Model for the 1975 Pocatello Valley Earthquake," Systems, Science and Software Report AFGL-TR-79-0001 submitted to the Air Force Geophysics Laboratory, December.

Hoffman, H. V. and F. M. Sauer (1969), "Free Field and Surface Motions, PILEDRIVER Event," Stanford Research Institute Report POR 4000.

Ida, Y. (1972), "Cohesive Force Across the Tip of a Longitudinal-Shear Crack and Griffith's Specific Surface Energy," J. Geophys. Res., Vol. 77, pp. 3796-3805.

Perret, W. R. (1968), "Free Field Ground Motion in Granite, PILEDRIVER Event," Sandia Corporation Report POR-4001.

Springer, D., M. Denny, J. Healy and V. Mickey (1968), "The STERLING Experiment: Decoupling of Seismic Waves by a Shot-Generated Cavity," J. Geophys. Res., 73, 18, September.